nature nanotechnology

LETTERS

PUBLISHED ONLINE: 25 MARCH 2012 | DOI: 10.1038/NNANO.2012.37

Observation of quantum interference in molecular charge transport

Constant M. Guédon[1†], Hennie Valkenier[2†], Troels Markussen[3], Kristian S. Thygesen[3], Jan C. Hummelen[2] and Sense Jan van der Molen[1*]

As the dimensions of a conductor approach the nanoscale, quantum effects begin to dominate, and it becomes possible to control the conductance through direct manipulation of the electron wavefunction. Such control has been demonstrated in various mesoscopic devices at cryogenic temperatures[1–4], but it has proved to be difficult to exert control over the wavefunction at higher temperatures. Molecules have typical energy level spacings (∼eV) that are much larger than the thermal energy at 300 K (∼25 meV), and are therefore natural candidates for such experiments. Previously, phenomena such as giant magnetoresistance[5], Kondo effects[6] and conductance switching[7–11] have been observed in single molecules, and theorists have predicted that it should also be possible to observe quantum interference in molecular conductors[12–18], but until now all the evidence for such behaviour has been indirect. Here, we report the observation of destructive quantum interference in charge transport through two-terminal molecular junctions at room temperature. We studied five different rigid π-conjugated molecular wires, all of which form self-assembled monolayers on a gold surface, and find that the degree of interference can be controlled by simple chemical modifications of the molecular wire.

The conductance properties of solid-state mesoscopic structures are dominated by quantum effects at low temperatures. For example, if partial electron waves propagating through the two branches of a ring-shaped mesoscopic structure interfere with each other destructively, conductance is suppressed, and if they interfere constructively, conductance is enhanced[1,4]. Similar behaviour is expected to occur for certain classes of molecular junctions[13–19], with the interference occurring between electron waves propagating through molecular orbitals that are separated in both space and energy. Because the properties of molecular orbitals can be manipulated by chemical design, it should be possible to tune the conductance of single-molecule junctions over orders of magnitude at ambient temperatures. Although variations in charge-transfer rates within donor–bridge–acceptor molecules can be explained in terms of interference[20,21], until now, all the evidence for quantum interference in molecular conductance experiments has been indirect[22–24]. Here, we provide direct evidence for destructive quantum interference in two-terminal molecular junctions.

To investigate the influence of quantum interference on molecular conductance properties, we synthesized five rigid π-conjugated molecular wires (see Supplementary Information). The first two molecules (AQ-MT and AQ-DT; Fig. 1a, left) contain an anthraquinone unit. This makes them cross-conjugated[25]. The AQ-MT molecule is terminated by a protected thiol group at one side only (monothiolated, MT), whereas AQ-DT is dithiolated (DT). The third molecular wire (AC-DT) contains a central anthracene unit and is linearly conjugated. Otherwise it is very similar to AQ-DT (for example, both have a length of 24.5 Å). Finally, two linearly conjugated reference compounds—oligo(phenylene–ethynylene)-monothiol and -dithiol (OPE3-MT and OPE3-DT)—were studied. We stress that apart from the thiols, all five molecules have the same phenylene–ethynylene endgroups.

To measure charge transport, we first created self-assembled monolayers (SAMs) of each molecule type on thin gold layers (200 nm, on silicon substrates). To obtain high-quality, densely packed SAMs, we used a procedure established recently (see Supplementary Information)[26]. Next, a conducting atomic force microscopy (AFM) probe was brought into close contact with a SAM. In this way, we were able to perform charge-transport experiments through the molecular layer, using the gold-covered substrate and the AFM tip as electrodes (Fig. 1b). We typically connected to a few hundred molecules while measuring current I versus bias voltage V (ref. 27). However, the exact number varied. For this reason, we present our results as two-dimensional histograms. Figure 1c shows such a two-dimensional histogram for AC-DT. To construct this plot, we logarithmically binned the dI/dV values (determined numerically) for each bias applied (see Supplementary Information). This effectively results in a sequence of one-dimensional histograms, plotted for each V. To illustrate this, Fig. 1d presents a cross-section of Fig. 1c at $V = 0$ V (blue histogram, corresponding to the dashed line in Fig. 1c). This is the zero-bias one-dimensional histogram for AC-DT[28]. Representing our data in two-dimensional histograms has two major advantages. First, it allows us to show a full data set in one plot, without a need for either determining an average curve or for data selection[28] (see Supplementary Information). Second, it enables us to distinguish general tendencies in the dI/dV curves from statistical variations in the conductance values themselves. The latter are inherent to molecular transport studies[27,28]. Figure 1c clearly illustrates this advantage: a symmetric valley-like shape is seen for the full data range. This shape is virtually independent of the conductance values, which do scatter (Fig. 1d).

Figure 1d compares the zero-bias conductance histograms for AQ-DT (red) and AC-DT (blue). Interestingly, AQ-DT exhibits conductance values that are almost two orders of magnitude lower than those of AC-DT. This is quite remarkable, because the energy difference between the highest occupied molecular orbital (HOMO) and lowest unoccupied molecular orbital (LUMO) levels is very similar for these molecules. From ultraviolet–visible measurements, we find an optical HOMO–LUMO gap of 2.88 eV

[1]Kamerlingh Onnes Laboratorium, Leiden University, Niels Bohrweg 2, 2333 CA Leiden, The Netherlands, [2]Stratingh Institute for Chemistry and Zernike Institute for Advanced Materials, University of Groningen, Nijenborgh 4, 9747 AG Groningen, The Netherlands, [3]Center for Atomic-scale Materials Design (CAMD), Department of Physics, Technical University of Denmark, DK-2800 Kgs. Lyngby, Denmark, †These authors contributed equally to this work. *e-mail: molen@physics.leidenuniv.nl

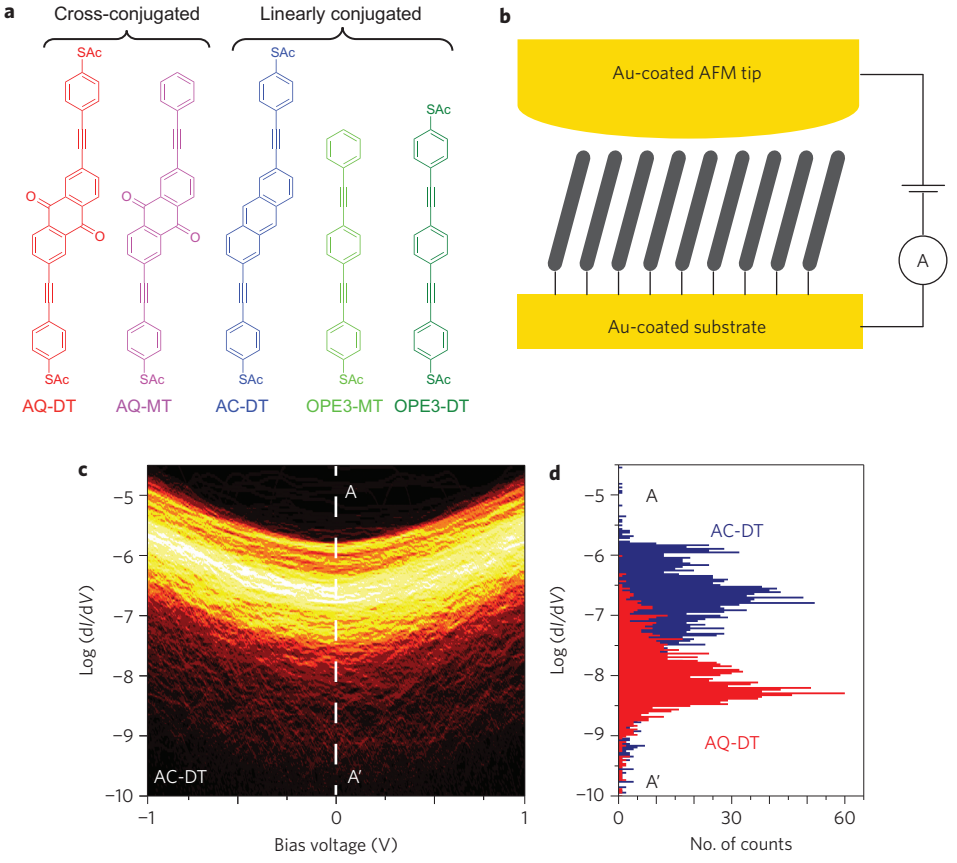

Figure 1 | Conductance measurements on molecular wires. a, Chemical structure of the molecules. AQ-DT and AQ-MT are both cross-conjugated, whereas AC-DT, OPE3-DT and OPE3-MT are linearly conjugated. AQ-DT, AC-DT and OPE3-DT are dithiolated and thus symmetric. AQ-MT and OPE3-MT are monothiolated. The colour code is also used in the following figures. **b**, Schematic view of the junction formed by the molecules self-assembled on a conducting substrate (gold) and the conducting AFM tip (gold). **c**, Logarithmically binned two-dimensional histogram for dI/dV values versus bias voltage V for AC-DT (in Ω^{-1}); the colour scale indicates the number of counts (black, no counts; white, more than 40 counts). **d**, Cross-section of the two-dimensional histogram shown in **c** along line A–A′ (zero-bias conductance) resulting in a one-dimensional histogram (blue). A one-dimensional histogram for AQ-DT taken from Fig. 3a is shown in red.

for AQ-DT and 2.90 eV for AC-DT. Our density functional theory (DFT) calculations (see Supplementary Information) yield fundamental HOMO–LUMO gaps of 4.23 eV and 4.61 eV, respectively. (Note that the optical gap and the fundamental gap differ by the electron–hole interaction.) Furthermore, Fig. 1d cannot be trivially explained from a weaker coupling of AQ-DT to the AFM tip, because the endgroups of both molecules are the same. As we shall elaborate below, the large difference in conductance is instead indicative of destructive interference in the AQ-DT junctions. In Fig. 2a we present calculations of the energy-dependent transmission function, $T(E)$, for junctions containing AC-DT, AQ-DT and AQ-MT. This function describes the quantum-mechanical probability that an electron with energy E traverses the molecular junction. Once $T(E)$ is known, the $I(V)$ curves can be calculated using Landauer's formula (see Supplementary Information). In particular, the low bias conductance is given by $\mathrm{d}I/\mathrm{d}V(V=0) = 2e^2/h \cdot T(E=E_F)$. For a molecular junction, $T(E)$ typically exhibits peaks around the orbital energies, where electrons can tunnel resonantly. In the energy gaps, $T(E)$ is normally rather featureless, as exemplified by AC-DT in Fig. 2a. However, for AQ-DT and AQ-MT, $T(E)$ exhibits a strong dip or 'anti-resonance'. This feature is a result of destructive interference[13–19]. To reveal the origin of the anti-resonance, we transformed the frontier molecular orbitals into an equivalent set of maximally localized molecular orbitals (LMOs)[16]. The upper part of Fig. 2d shows the three relevant LMOs obtained for AQ-DT. Two are localized on the left and right parts of the AQ-DT, respectively. These LMOs have the same energy and correspond essentially to the sum and difference of the almost degenerate HOMO and HOMO–1 (Fig. 2a). The LMO localized in the centre of AQ-DT is essentially the LUMO and has a higher energy. It is now clear that an electron with energy E lying inside the HOMO–LUMO gap can traverse the molecule by means of two distinct paths: directly from the left to the right LMO, or via the energetically higher LMO (arrows in Fig. 2d). It can be shown that the upper and lower routes yield a phase difference of π within the HOMO–LUMO gap; that is, the partial waves interfere destructively (see Supplementary Information). Consequently, $T(E)$ shows a strong minimum at the energy where the partial waves have equal weight. Figure 2c illustrates this, by showing $T(E)$ calculated for the lower and upper routes separately, as well as for the combined three-site model. Note the similarity to Fig. 2a. For AC-DT, the HOMO is well separated from HOMO–1. Hence, a transformation to LMOs leads to only two, left and right localized orbitals (Fig. 2b). As there is only a single path available, no interference effects occur for AC-DT.

We now compare these calculations with the experiments in Fig. 1d. In Fig. 2a, the $T(E_F)$ values are approximately two orders of magnitude lower for AQ-DT than for AC-DT. This is in reasonable agreement with the strongly reduced conductance values for AQ-DT in Fig. 1d. We thus have a first indication of interference in AQ-DT. To investigate this further, we inspect the full two-dimensional histogram of AQ-DT (Fig. 3a). For the full voltage

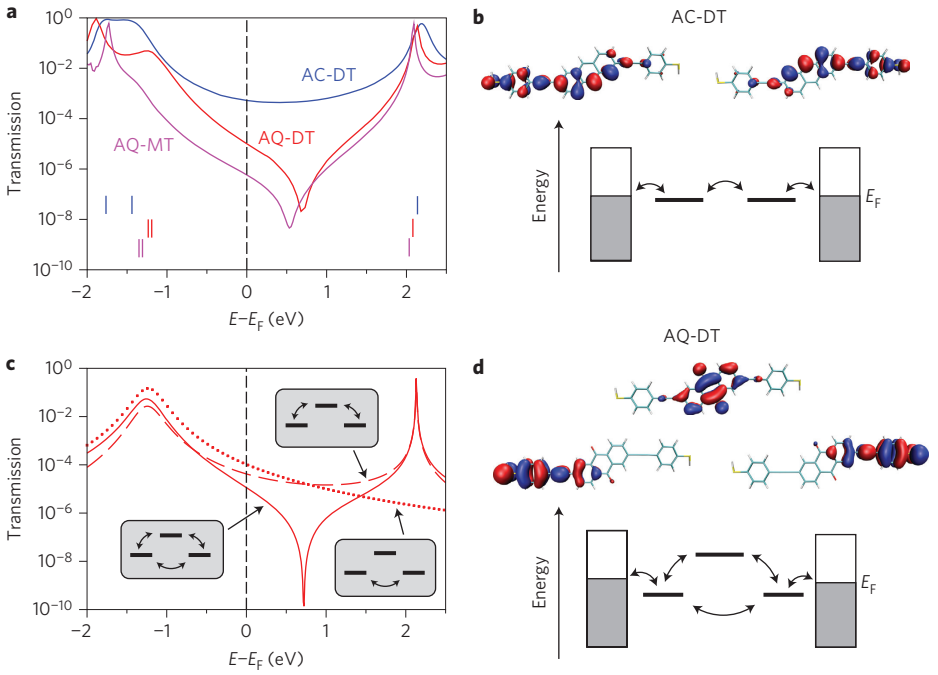

Figure 2 | Origin of interference in cross-conjugated molecules. a, Transmission functions $T(E)$ for AC-DT (blue), AQ-DT (red) and AQ-MT (purple) calculated with DFT + Σ. Vertical bars mark the energies of the frontier orbitals HOMO–1, HOMO (left side) and LUMO (right side). **b**,**d**, The lower parts show schematic transport models derived from the localized molecular orbitals presented in the upper parts (AC-DT, **b**; AQ-DT, **d**). In the three-site model shown in **d**, there are evidently two routes through the molecule: a lower route directly from the left to the right site and an upper route via the central orbital. **c**, $T(E)$ for the lower (dotted line) and upper (dashed line) route in **d**. A coherent addition of the transmission probability amplitudes from the two paths, with a phase difference of π, yields the three-site transmission function (solid line). This reproduces the essential features of **a**, for AQ-DT and AQ-MT.

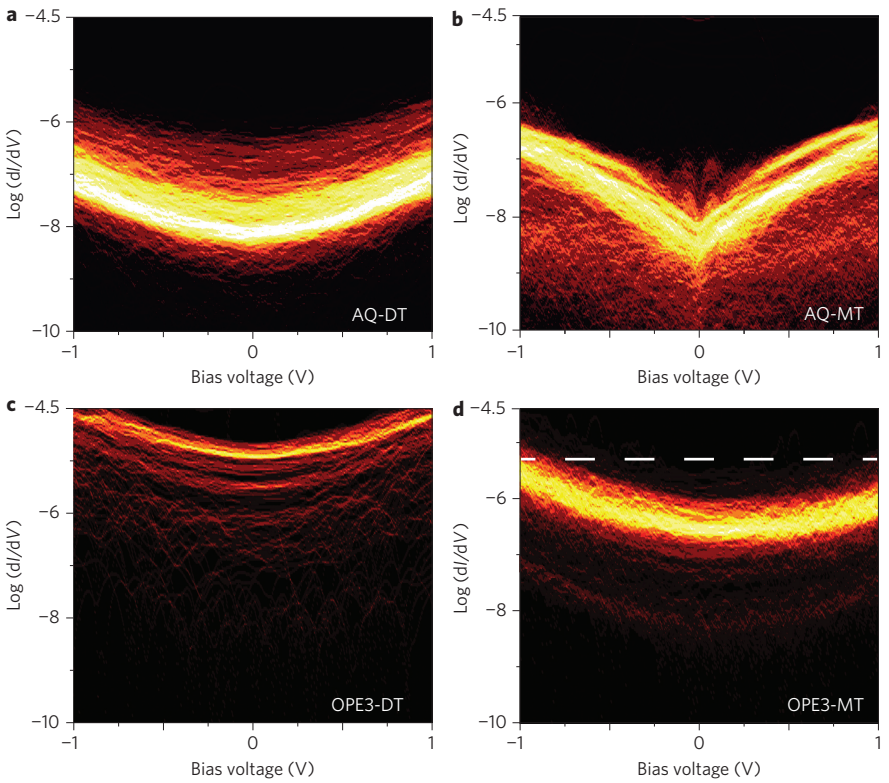

Figure 3 | Two-dimensional conductance histograms. a–d, Logarithmically binned two-dimensional histograms of dI/dV (in Ω^{-1}) versus bias voltage V for AQ-DT (**a**), AQ-MT (**b**), OPE3-DT (**c**) and OPE3-MT (**d**). The colour scale indicates the number of counts and ranges from black (0 counts) to white (more than 40 counts). In **d**, a dashed line visualizes the asymmetry in the dI/dV curves of OPE3-MT, resulting from asymmetric coupling. Corresponding molecular structures are shown in Fig. 1a.

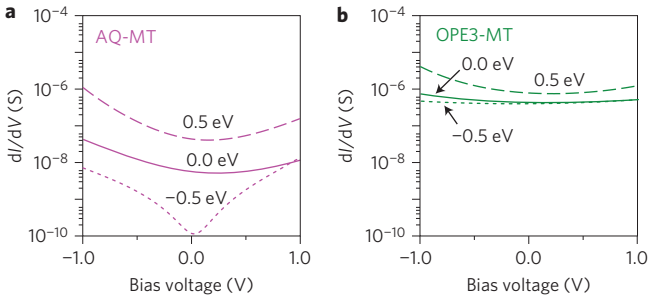

Figure 4 | Calculated d*I*/d*V* curves for AQ-MT and OPE3-MT. **a**, dI/dV for AQ-MT, computed from the transmission function in Fig. 2a. $T(E)$ was shifted by $\Delta E = 0.0$ eV, $\Delta E = 0.5$ eV and $\Delta E = -0.5$ eV, relative to E_F. We include asymmetry in the bias drop by means of parameter $\eta = 0.6$ (see Supplementary Information). To account for multiple molecules contacting the AFM tip, we have multiplied the transmission function by a factor of 100. For $\Delta E = -0.5$ eV both the shape and range of dI/dV, spanning two orders of magnitude, are in excellent agreement with experiments (Fig. 3b). **b**, Similar calculation for OPE3-MT. Asymmetric curves and higher conductance values with smaller variation are found, consistent with Fig. 3d.

range, its dI/dV values are dramatically lower than those of AC-DT (Fig. 1c). However, the two-dimensional histogram has a parabola-like appearance similar to AC-DT; that is, we observe no anomaly that can be connected to the calculated transmission dip. Hence, although the surprisingly low conductance of AQ-DT is most probably due to quantum interference, the evidence is only indirect. This situation is comparable to that in refs 22–24.

Let us next consider AQ-MT molecules, which should also exhibit an anti-resonance (Fig. 2a). Figure 3b shows the two-dimensional histogram of the dI/dV curves for AQ-MT (see Supplementary Information). Remarkably, these data do show a clear anomaly at zero bias voltage. In particular, the curvature of the dI/dV traces in Fig. 3b is negative for all V (except around $V = 0$). What is equally striking in Fig. 3b is the large voltage range over which the anomaly extends. Even up to $V = \pm 1$ V, the dI/dV curves are dominated by the minimum at $V = 0$ V. This points to a characteristic energy scale of ~1 eV, which corresponds well with the width of the interference-induced dip in $T(E)$ in Fig. 2a. Moreover, this large energy scale rules out Kondo effects and Coulomb blockade as possible explanations for the anomaly (see Supplementary Information). Hence, Fig. 3b makes a strong case for quantum interference.

To further validate this interpretation, we calculated dI/dV curves for AQ-MT from $T(E)$ (see Supplementary Information). A key role in these calculations is played by the position of the anti-resonance in $T(E)$ relative to E_F. This position is difficult to predict theoretically. This is related to the well-known problems of the applied methodology to describe energy level alignments and to the uncertainty of the size of the surface dipoles in the experiments. The position of the anti-resonance is particularly sensitive to such effects due to the low density of states in the HOMO–LUMO gap (see fig. 5 in ref. 23). It is thus reasonable to treat the position of the transmission minimum as a free variable within a limited energy window. Figure 4a presents dI/dV curves for AQ-MT, calculated for three cases: no energy shift (compared to Fig. 2a) and shifts of ± 0.5 eV. We take into account that AQ-MT molecules are probed asymmetrically. For a shift of -0.5 eV, the calculated dI/dV characteristic is in remarkable agreement with the measured curves in Fig. 3b. The negative curvature is reproduced, and the voltage scale and the range of dI/dV values over which the minimum extends agree. Finally, the dI/dV curves are nearly symmetric in both calculation and experiment. This latter point is indeed noteworthy, because AQ-MT is contacted asymmetrically. The symmetry in Fig. 3b must therefore be a consequence of $T(E)$ being symmetric around E_F or, equivalently, of E_F lying near the interference minimum. To independently confirm that monothiols are asymmetrically coupled, we also measured dI/dV curves for OPE3-DT (Fig. 3c) and OPE3-MT (Fig. 3d). As expected, symmetric data are obtained for OPE3-DT, whereas asymmetric dI/dV curves are found for OPE3-MT (see Fig. 4b for calculated results). Hence, we conclude that Fig. 3b constitutes direct evidence for quantum interference in AQ-MT molecular junctions.

The question remains why AQ-DT does not show a zero-bias anomaly, despite its suppressed conductance values. This is related to charge transfer. AQ-DT junctions comprise two gold–sulphur dipoles, whereas AQ-MT junctions have only one. Hence, for AQ-DT, the transmission dip is shifted to higher energies than for AQ-MT; that is, it will lie above E_F. Consequently, its dI/dV curves show no anomaly (Fig. 4a and see Supplementary Information).

In summary, our charge-transport data on cross-conjugated anthraquinone derivatives are fully consistent with destructive quantum interference in molecular junctions. The interference effects are intimately linked to the shapes and energies of the molecular orbitals and can thus be controlled by chemical design. The fact that interference in molecules is present at room temperature opens the road to a new type of molecular device. Specifically, these include interference-controlled molecular switches with very large on–off ratios[11,25] and novel thermoelectric devices, with thermopower values tunable in magnitude and sign[29].

Methods

Samples were prepared by thermal deposition of 5 nm chromium and 200 nm gold onto silicon/silicon oxide substrates. These freshly prepared samples were immediately transferred into a nitrogen-filled glovebox. The molecular wires were dissolved in dry chloroform (AC-DT, AQ-DT, AQ-MT) or in dry tetrahydrofuran (THF) (OPE3-DT and OPE3-MT) at 0.5 mM in this glovebox. We added 10% (v/v) degassed triethylamine to these solutions to deprotect the thiol groups and immersed the gold samples for 2 days to form densely packed SAMs[26] as confirmed by ellipsometry and X-ray photoelectron spectroscopy (XPS) (see Supplementary Information). After immersion, the samples were rinsed three times with clean chloroform or THF, and dried in the glovebox. The synthesis of AQ-MT and the characterization of all five molecular wires is reported in the Supplementary Information. Transport experiments were performed on a Digital Instrument Multimode-AFM with a Nanoscope III controller. The conductance measurements themselves were controlled externally (see Supplementary Information). Calculations of junction geometries and transmission functions were performed with the GPAW DFT code using an atomic orbital basis set corresponding to double-zeta plus polarization and the Perdew–Burke–Ernzerhof exchange-correlation functional. Before calculating the transmission functions, the occupied and unoccupied molecular orbitals were shifted in energy to account for self-interaction errors and missing image charge effects in the DFT description. This approach (DFT + Σ) was recently found to systematically improve the DFT conductance values[30] (see Supplementary Information).

Received 27 October 2011; accepted 21 February 2012; published online 25 March 2012

References

1. Webb, R. A., Washburn, S., Umbach, C. P. & Laibowitz, R. B. Observation of h/e Aharonov–Bohm oscillations in normal-metal rings. *Phys. Rev. Lett.* **54,** 2696–2699 (1985).
2. van Wees, B. J. *et al.* Quantized conductance of point contacts in a two-dimensional electron gas. *Phys. Rev. Lett.* **60,** 848–850 (1988).
3. Wharam, D. A. *et al.* One-dimensional transport and the quantisation of the ballistic resistance. *J. Phys. C* **21,** L209–L214 (1988).
4. Beenakker, C. W. J. & van Houten, H. Quantum transport in semiconductor nanostructures. *Solid State Phys.* **44,** 1–228 (1991).
5. Schmaus, S. *et al.* Giant magnetoresistance through a single molecule. *Nature Nanotech.* **6,** 185–189 (2011).
6. Park, J. *et al.* Coulomb blockade and the Kondo effect in single-atom transistors. *Nature* **417,** 722–725 (2002).
7. Smit, R. H. M. *et al.* Measurement of the conductance of a hydrogen molecule. *Nature* **419,** 906–909 (2002).
8. Kubatkin, S. *et al.* Single-electron transistor of a single organic molecule with access to several redox states. *Nature* **425,** 698–701 (2003).

9. Venkataraman, L. *et al.* Single-molecule circuits with well-defined molecular conductance. *Nano Lett.* **6,** 458–462 (2006).
10. Mishchenko, A. *et al.* Influence of conformation on conductance of biphenyl-dithiol single-molecule contacts. *Nano Lett.* **10,** 156–163 (2010).
11. Van der Molen, S. J. & Liljeroth, P. Charge transport through molecular switches. *J. Phys. Condens. Matter* **22,** 133001 (2010).
12. Sautet, P. & Joachim, C. Electronic interference produced by a benzene embedded in a polyacetylene chain. *Chem. Phys. Lett.* **153,** 511–516 (1988).
13. Andrews, D. Q., Solomon, G. C., Van Duyne, R. P. & Ratner, M. A. Single molecule electronics: increasing dynamic range and switching speed using cross-conjugated species. *J. Am. Chem. Soc.* **130,** 17309–17319 (2008).
14. Stafford, C. A., Cardamone, D. M. & Mazumdar, S. The quantum interference effect transistor. *Nanotechnology* **18,** 424014 (2007).
15. Ernzerhof, M., Zhuang, M. & Rocheleau, P. Side-chain effects in molecular electronic devices. *J. Chem. Phys.* **123,** 134704 (2005).
16. Markussen, T., Stadler, R. & Thygesen, K. S. The relation between structure and quantum interference in single molecule junctions. *Nano Lett.* **10,** 4260–4265 (2010).
17. Markussen, T., Schiotz, J. & Thygesen, K. S. Electrochemical control of quantum interference in anthraquinone-based molecular switches. *J. Chem. Phys.* **132,** 224104 (2010).
18. Solomon, G. C., Herrmann, C., Hansen, T., Mujica, V. & Ratner, M. A. Exploring local currents in molecular junctions. *Nature Chem.* **2,** 223–228 (2010).
19. Yaliraki, S. & Ratner, M. Interplay of topology and chemical stability on the electronic transport of molecular junctions. *Ann. NY Acad. Sci.* **960,** 153–162 (2002).
20. Patoux, C., Coudret, C., Launay, J. P., Joachim, C. & Gourdon, A. Topological effects on intramolecular electron transfer via quantum interference. *Inorg. Chem.* **36,** 5037–5049 (1997).
21. Ricks, A. B. *et al.* Controlling electron transfer in donor-bridge-acceptor molecules using cross-conjugated bridges. *J. Am. Chem. Soc.* **132,** 15427–15434 (2010).
22. Mayor, M. *et al.* Electric current through a molecular rod—relevance of the position of the anchor groups. *Angew. Chem. Int. Ed.* **42,** 5834–5838 (2003).
23. Fracasso, D., Valkenier, H., Hummelen, J. C., Solomon, G. C. & Chiechi, R. C. Evidence for quantum interference in SAMs of arylethynylene thiolates in tunneling junctions with eutectic GaIn (EGaIn) top-contacts. *J. Am. Chem. Soc.* **133,** 9556–9563 (2011).
24. Hong, W. *et al.* An MCBJ case study: the influence of π-conjugation on the single-molecule conductance at a solid/liquid interface. *Beilstein J. Nanotechnol.* **2,** 699–713 (2011).
25. Van Dijk, E. H., Myles, D. J. T., van der Veen, M. H. & Hummelen, J. C. Synthesis and properties of an anthraquinone-based redox switch for molecular electronics. *Org. Lett.* **8,** 2333–2336 (2006).
26. Valkenier, H. *et al.* Formation of high-quality self-assembled monolayers of conjugated dithiols on gold: base matters. *J. Am. Chem. Soc.* **133,** 4930–4939 (2011).
27. Wold, D. J. & Frisbie, C. D. Fabrication and characterization of metal–molecule–metal junctions by conducting probe atomic force microscopy. *J. Am. Chem. Soc.* **123,** 5549–5556 (2001).
28. Gonzalez, M. T. *et al.* Electrical conductance of molecular junctions by a robust statistical analysis. *Nano Lett.* **6,** 2238–2242 (2006).
29. Bergfield, J. P. & Stafford, C. A. Thermoelectric signatures of coherent transport in single-molecule heterojunctions. *Nano Lett.* **9,** 3072–3076 (2009).
30. Quek, S. Y., Choi, H. J., Louie, S. G. & Neaton, J. B. Length dependence of conductance in aromatic single-molecule junctions. *Nano Lett.* **9,** 3949–3953 (2009).

Acknowledgements

The authors thank T. Oosterkamp and F. Galli for making their equipment and expertise available, J. van Ruitenbeek and M. Trouwborst for discussions and D. Myles for his initial synthetic efforts. This study was financed by a VIDI grant (to S.J.vdM.) from the Netherlands Organization for Scientific Research (NWO), by the Dutch Ministry of Economic Affairs via NanoNed (to H.V., project GMM.6973), by the FTP (grant no. 11-104592 to T.M.) and The Sapere Aude program under the Danish Council for Independent Research (grant no. 11-105139 to K.S.T.).

Author contributions

C.M.G., H.V. and S.J.vdM. performed AFM measurements and carried out data analysis. H.V. and J.C.H. designed and synthesized the molecules, and made and characterized the SAMs. T.M. and K.S.T. performed the calculations. C.M.G., H.V., J.C.H. and S.J.vdM. designed the experiment. All authors discussed the results and commented on the manuscript.

Additional information

The authors declare no competing financial interests. Supplementary information accompanies this paper at www.nature.com/naturenanotechnology. Reprints and permission information is available online at http://www.nature.com/reprints. Correspondence and requests for materials should be addressed to S.J.v.d.M.